FULL PAPER

Tailoring Microstructure of Graphene-Based Membrane by Controlled Removal of Trapped Water Inspired by the Phase Diagram

*Wei Lv, Zhengjie Li, Guangmin Zhou, Jiao-Jing Shao, Debin Kong, Xiaoyu Zheng, Baohua Li, Feng Li, Feiyu Kang, and Quan-Hong Yang**

As an important form of graphene assembled in macroscale, the graphene-based membrane attracts much attention due to its easy manipulation and various potential applications. However, tailoring the microstructure of these membranes is hard to achieve and the surface utilization of graphene layers is low. By analyzing the drying process for the wet graphene oxide membrane (GOM), it is found that the trapped water in freshly formed GOM actually provides potential forces to tune its microstructure. According to the phase diagram of pure water, with a reduced pressure, the trapped water boils seriously and then transforms into ice crystal instantaneously around the triple point. This sudden phase change across the triple point provides strong forces to change and fix the microstructure of GOM. In this study, the ordinary evaporation drying process for the wet GOM is replaced with a two-stage drying process and the tightly layered structure of graphene membrane is turned into an open and grade structure. The obtained membrane shows high surface utilization. Thus, after reduction, the membrane possesses high adsorption capability towards various molecules, especially for heavy oil and lithium polysulfide products in the cathode of Li–S battery. Furthermore, the membrane shows high rate performance as the electrodes for supercapacitors.

1. Introduction

Macroscopic freestanding membrane is one of the most important forms of assembled graphene and has attracted great attention in recent years due to their flexibility and unique properties inherited from graphene.[1] Recently, membrane-like energy storage devices have become one of the hottest topics of graphene research, in which a graphene-based membrane is used as the flexible electrode due to its easy preparation and manipulation.[2] However, the electrolyte ions are often limited from penetrating inside the closely stacked membrane electrode because the ion transportation direction is perpendicular to the layer orientation.[3] Moreover, the closely stacked structure provides a low graphene surface availability, limiting the energy density improvement.[4] Such a closely stacked structure also restricts the applications of graphene membranes in other fields, such as filtration and adsorption-derived applications. Thus, tailoring the microstructure of the graphene-based membrane is an urgent issue. Recent reports have shown that the closely stacked structure can be loosened to some extent by introducing spacers between graphene layers, but the layer orientation cannot yet be well controlled.[2d,5] Very recently, water and some other liquids have been proven as the important components to tune the microstructure and properties of graphene-based assemblies. The water or some other liquids trapped in the formed graphene-based assembly or dispersion can be used to construct metastable and adaptive pore structure, in which the stacking of the graphene sheets is optimized to reach desirable properties, such as high packing density or ordered sheet arrangement.[4,6] In our previous study, we have successfully prepared a three-dimensional graphene assembly with a high density and ultrahigh electrochemical volumetric capacitance by precisely controlling the removal process of trapped water.[7]

A graphene oxide membrane (GOM) is a typical form of graphene-based membrane, and two methods, filtration and liquid/air assembly, are the normally used strategies for its fabrication.[1a,8] When freshly removed from the hydrosol, the GOM, which is assembled at the liquid/air interface, contains a certain amount of water before further drying, and a layered structure is formed when the water evaporates slowly in atmospheric or vacuum environments.[8a] In this case, the water trapped between the adjacent layers is vaporized and released

Dr. W. Lv, Prof. B. H. Li, Prof. F. Y. Kang, Prof. Q.-H. Yang
Engineering Laboratory for Functionalized Carbon Materials, Graduate School at Shenzhen
Tsinghua University
Shenzhen 518055, P. R. China
E-mail: yang.quanhong@mail.sz.tsinghua.edu.cn
Z. J. Li, J.-J. Shao, D. B. Kong, X. Y. Zheng, Prof. Q.-H. Yang
School of Chemical Engineering and Technology
Tianjin University
Tianjin 300072, P. R. China
E-mail: qhyangcn@tju.edu.cn
G. M. Zhou, Prof. F. Li
Shenyang National Laboratory for Materials Science
Institute of Metal Research
Chinese Academy of Sciences
Shenyang 110016, P. R. China

DOI: 10.1002/adfm.201304054

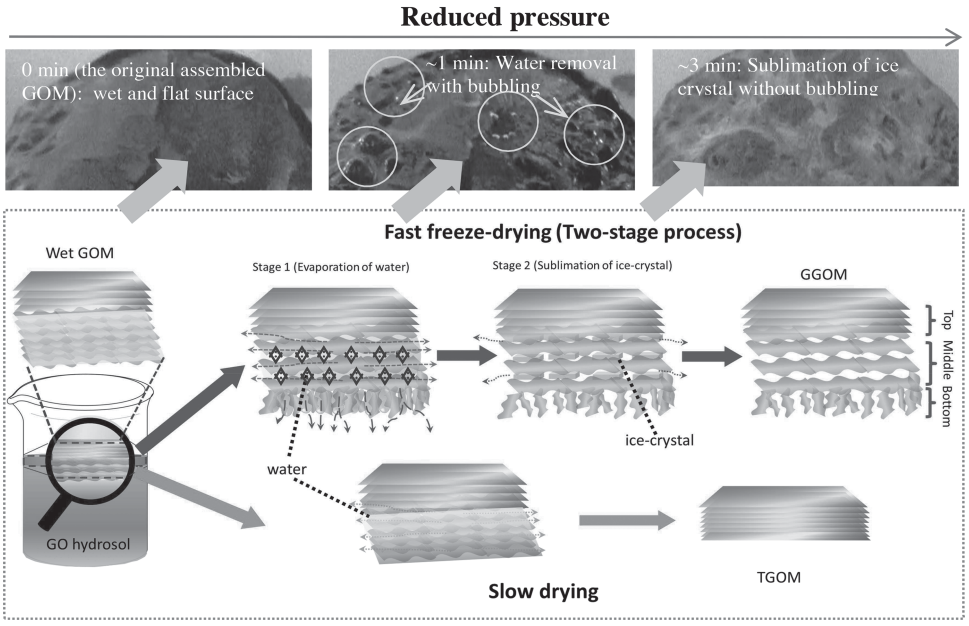

Figure 1. Schematic of the formation processes of the closely stacked microstructure (for TGOM) and open and graded microstructure (for GGOM) in a graphene oxide membrane (GOM) self-assembled at the liquid/air interface. The upper digital photos show the changes (with drying time) of the bottom side of the membrane during the two-stage drying process with reduced pressure.

sideways from the membrane and a GOM with tightly layered structure (denoted as TGOM) is naturally formed, as schematically shown in **Figure 1** (lower). Inspired by an analysis of the layered structure formation process, we consider that the removing process of water trapped actually may provide a driving force to finely tune the stacking state and orientation of graphene layer in a GOM.

The drying of the membrane, in other words, the removal of the trapped water from the layered structure, is intrinsically a transition from a liquid to gaseous state. Water may transform to gaseous state in two ways, vaporization from liquid water as described above to form TGOM and sublimation from frozen water (ice) with a pre-freezing process. The two ways in which water are removed may give different driving forces to tune the microstructure of the formed GOM. In the evaporation-dominated drying process, the relatively strong interaction between water and graphene oxide sheets is the main cause for the tightly stacked structure in the resultant GOM while,[7,9] in the sublimation-dominated drying process, the resultant GOM possesses a slightly loosened layer structure since the trapped water has already been frozen into ice before drying and graphene oxide sheets are separated from the ice.[6a,10]

Generally, limited force is generated during the slow vaporization of liquid-state water in an evaporation induced drying process or sublimation of the frozen water (ice) in an ordinary freeze-drying process. According to the phase diagram of a pure substance (Figure S1, Supporting Information), at reduced pressure and decreasing temperature, water may transform to gaseous state in two successive processes, vaporization from liquid water above the triple point and sublimation from frozen water (ice) below the triple point. That means, near the triple point, water may endure severe and sudden phase changes across the three phases (water, vapor, and ice), and such instantaneous phase changes may provide a strong driving force to tune the microstructure of the finally formed membrane (orientation and stacking state of graphene sheets).

In this study, we use a freeze-drier to realize the above two-stage drying process across the triple point by reducing the pressure. In contrast to an ordinary freeze-drying where pre-frozen sample is required to fix the microstructure of water-rich samples, in the two-stage process, a wet sample with abundant trapped water is directly put into the freeze-drier and endures a fast evaporation of liquid water at reduced pressure inducing a fast decreasing of temperature, that is followed by a sublimation of a small amount of frozen ice at very low temperature. Accordingly, a GOM with a graded structure and vertical openings at bottom side (denoted as GGOM) is obtained, which is different from the closely stacked structure of TGOM, as illustrated in Figure 1. This membrane is described as a combination of three graded sections: a tightly layered structure (top), a loosely layered structure (middle) and vertically aligned sheets (bottom). The middle loosely layered structure and bottom vertical openings are accessible to foreign molecules. Note that such a graded structure can only be obtained in a membrane assembled at the liquid/air interface, not in the filtered membrane where the membrane is totally destroyed by the same two-stage drying owing to the absence of the upper tightly stacked structure, which helps maintain and fix the membrane morphology. The obtained membranes after reduction show high adsorption capability towards various molecules, especially for heavy oil and lithium polysulfide products in the cathode of Li–S battery. Furthermore, the membranes show high rate performance and cyclic stability when directly used as the electrodes for supercapacitors.

2. Results and Discussion

As illustrated in Figure 1, although with the same freeze-drier, the wet sample endures a two-stage drying that is entirely different from the ordinary freeze-drying in which the sublimation of the frozen water is the only process by which the trapped water is removed. That is, the two-stage drying process strictly follows the phase diagram in which the coexistence curves of different phases are demonstrated. With the decreasing pressure under a vacuuming process, the liquid water seriously boils that can be clearly observed in Figure S2 (Supporting Information), and after the pressure is low enough (reaching the triple point), the boiling water transformed into ice instantaneously and the boiling morphology of water is fixed. Considering the liquid-state water trapped between the graphene layers in GOM, two different phase changes hint us that the strong force generated from the boiling water can be used to change the closely stacked microstructure of GOM and the continuous phase change will help fix the changed structure.

In a typical formation process for a GGOM, a very thin film was first formed at the liquid/air interface and gradually assembled into a thicker membrane. The originally formed part (top) of the membrane, which was exposed to air, gradually dried forming a tightly layered structure during the continuing membrane formation. After the membrane was collected from interface, the lower part (below the dried thin film) in contact with the liquid still contained certain amount of water trapped among the adjacent graphene layers. Without a freezing pretreatment in liquid nitrogen as used for the ordinary freeze-drying, the freshly obtained wet GOM was then directly placed in a freeze-drier and subjected to a drying process with reduced pressure and decreasing temperature. The bottom side of GOM is wet and flat, which can be seen from Figure 1. That is, at the beginning of the drying at reduced pressure, the water molecules between the graphene layers were still in the liquid state (Figure S3, Supporting Information). As a result of fast vacuuming (reduced pressure) in the freeze-drier (Stage 1 shown in Figure 1), the water molecules between the graphene layers evaporated at a very high speed due to the fast drop of the boiling point at reduced pressure, and thus the bottom layers of the GOM were pulled vertically by the rapidly evaporating vapor flow while the interlayer distance in the middle part is expanded. Bubbles generated during the fast water removal process can be clearly observed on the bottom side of the assembled GOM as marked in the digital photo of Stage 1 shown in Figure 1. After the pressure was reduced enough to reach the triple point and the liquid water instantly transformed to ice crystals (Stage 2 indicated in Figure 1, and the color changes of the membrane is attributed to such transformation), which act as the spacers between the expanded graphene layers, subsequent sublimation removes the ice crystals in a direction parallel to the layers, and thus a loosely stacked structure was formed as a result of ice crystal removal. The digital photos shown in Figure 1 clearly show the different water removal processes.

A photo of the tailored freestanding GGOM is shown in **Figure 2**a, indicating that the membrane is flexible. Its open and graded structure is clearly indicated by the cross-sectional scanning electron microscopy (SEM) image shown in Figure 2b, from which three different sections (top, middle and bottom) can be clearly identified and the structure is totally different from that of TGOM dried at 70 °C in air (Figure S4, Supporting Information). A continuous thin film, which has tightly layered structure indicated by the SEM image in Figure 2c (Section 1), can be seen on the top of the GGOM (Figure 2c). This helps maintain the membrane morphology during the drying process with serve phase changes as mentioned above. The middle part of the GGOM (Section 2) shows an expanded and disordered structure due to the removal of ice crystals during the second-stage compared with the bottom part (Section 3) which

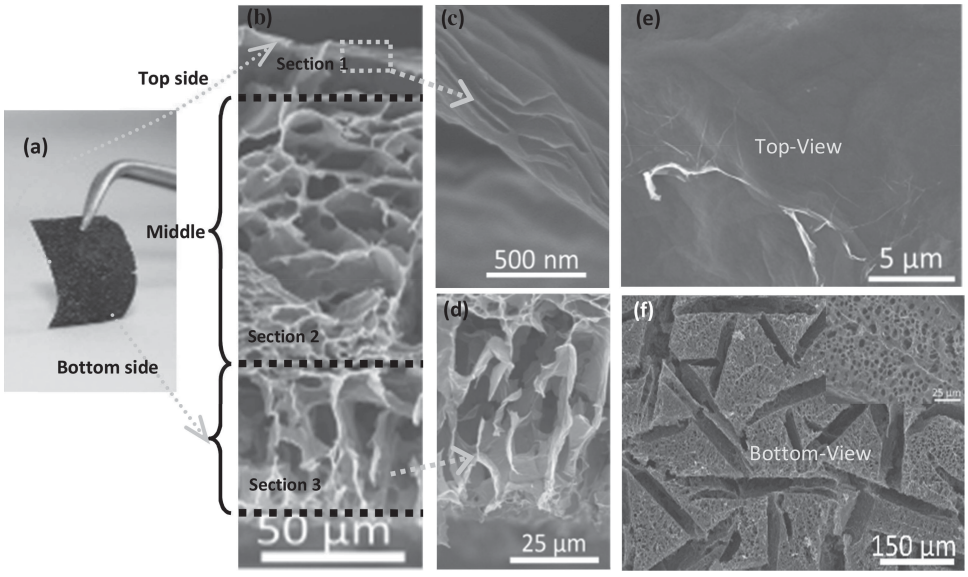

Figure 2. Open and graded microstructure of a GGOM. a) Photograph of a flexible GGOM; b) Cross-sectional SEM image of the membrane and c,d) the corresponding magnified images of the marked areas; e,f) top and bottom view SEM images of the membrane, and the overlay of (f) shows a magnified SEM image of the bottom.

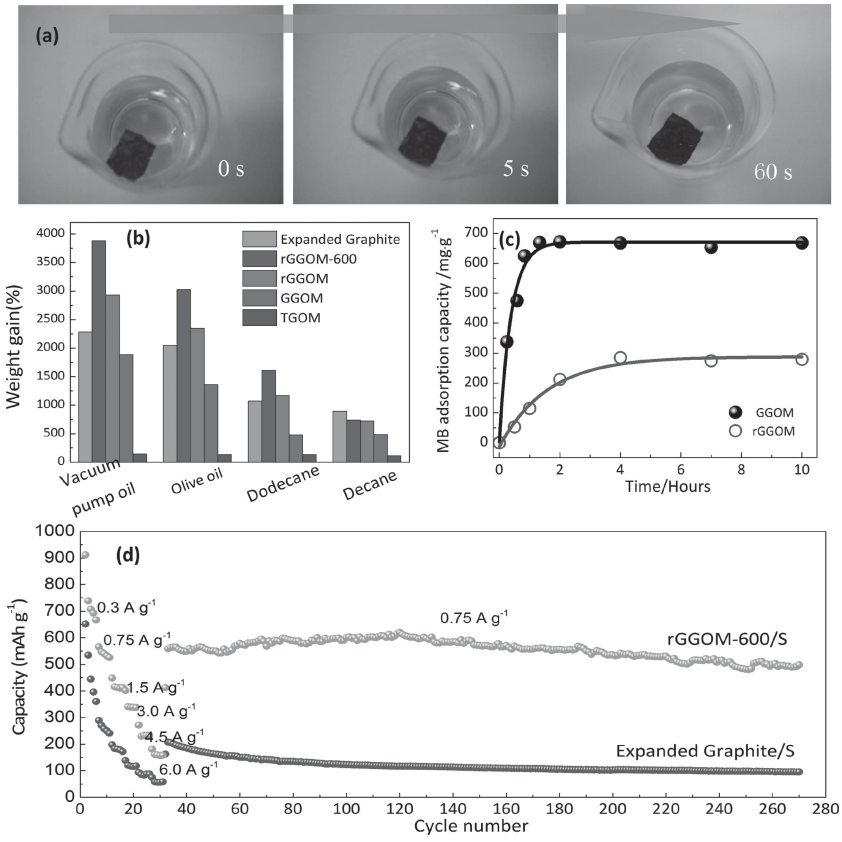

Figure 3. Adsorption and adsorption-related battery performance of GGOM. a) shows the fast adsorption of GGOM towards oil colored by Sudan II. b) The adsorption capacity of GGOM, reduced GGOM (rGGOM and rGGOM-600) and a reference expanded graphite towards various organics. c) Adsorption kinetics of the GGOM and rGGOM towards methylene blue (MB). d) The cyclic performance of the rGGOM-600/sulfur and expanded graphite/sulfur composites as the cathodes in Li–S batteries.

is the result of the strong forces caused by fast water removal that pull the layers into a vertical orientation during the first-stage drying as shown in Figure 1. Figure 2f shows the structure of the bottom of the membrane with large gaps and large macropores, which is totally different from the top flat surface with some ripples (Figure 2e and Figure S5, Supporting Information). In such a membrane, one quarter of graphene layers formed the layered structure in Section 1 which is roughly evaluated from the thickness comparison in Figure 2b (≈500 nm) and Supporting Information Figure S4 (≈2 μm for TGOM assembled with same period with GGOM), which can be used as an integrated current collector in the electrochemical applications resulting in a simple device assembly process. X-ray diffraction (XRD) patterns (Figure S6, Supporting Information) also indicate the structure difference of membranes subjected to different drying methods. TGOM shows a strong and sharp peak around 11° indicative of the tight stacking of the graphene oxide (GO) nanosheets, while only a small peak at about 11° with low intensity can be observed for GGOM. Since both of the membranes are assembled in the same conditions, the low intensity means that only a part of the GO nanosheets tightly restacked (Section 1), which is in accordance with the aforementioned structure discussion.

Such open and graded microstructure is relatively stable and cannot be changed during the reduction process, which can be proved by the XRD patterns shown in Figure S6. After the reduction using hydrazine hydrate vapor (denoted as rGGOM), the peak around 11° almost disappeared and a broader peak appeared at around 23°. After a following thermal treatment at 600 °C (denoted as rGGOM-600), the peak shifted to about 26° and became sharper, revealing that the GO was reduced to graphene and the layered structure revealed in Section 1 still exits. The specific surface areas of rGGOM and rGGOM-600 are 30–40 m^2 g^{-1} and 60–80 m^2 g^{-1} calculated by Brunauer-Emmett-Teller (BET) method respectively, which is far much higher than that of reduced TGOM (normally less than 5 m^2 g^{-1}).

Compared with TGOM, the graphene sheets in GGOM are more accessible to ions and molecules due to their open structure. Therefore, GGOM may have great potential as an absorbent, such as for dye and oil removal. Remarkably, the membrane can be directly used as a filtration membrane, and we designed a simple experiment to characterize its adsorption ability using methylene blue (MB) as a target molecule. As shown in Figure S7 in the Supporting Information, the GGOM displays a fast adsorption ability towards MB and the filtrate shows a much lighter color than the original solution containing a high MB concentration, and its adsorption capacity for MB is much higher (≈700 mg g^{-1}) than that of TGOM (≈200 mg g^{-1}). Heavy oil, like pump oil, is viscous and difficult to be adsorbed by microporous activated carbon,[11] the most frequently used adsorbent. GGOM displays fast and considerable adsorption ability towards heavy oil, as expected, because of its open structure and very large pores. As shown in **Figure 3**a, fast adsorption of vacuum pump oil (Ultra Grade 15 Oil, Edwards) which is colored by Sudan II (a kind of dye) for clear observation is revealed, and the oil surrounding the membrane is adsorbed as soon as the membrane touches it. GGOM shows a similar oil adsorption capacity to that of expanded graphite, an important adsorbent with large pores for oil removal (Figure 3b), and much higher capacity than TGOM due to its open structure. The aligned part (bottom) of the GGOM makes it easy for the oil to impregnate the membrane and be adsorbed, while the middle part provides large oil storage space. As GO is hydrophilic, it is difficult for the oil to impregnate the membrane, and this may restrict the oil adsorption capacity of GGOM. After chemical reduction (rGGOM) and further thermal treatment at 600 °C (rGGOM-600), the adsorption ability of the reduced GGOM towards oil is largely improved (Figure 3b). It is exciting to note that the reduced GGOM displays a much higher adsorption capacity for heavy oil (≈4000%) than for other organics

such as dodecane (≈2000%) and decane (≈1000%), showing great potential in environmental related applications. Although one quarter of graphene sheets cannot be utilized in the adsorption process, the adsorption capacity of rGGOM-600 is only slightly lower than that of the ultralight graphene foams reported recently with high layer utilization.[12] Another advantage is that the membrane morphology can be well maintained after adsorption process, which can be easily manipulated for the further treatment. Furthermore, the preparation process for such membrane is facile and fast, which ensures the mass production of the membrane in future practical applications.

Since the graded structure is not greatly changed during the mild reduction process, which is indicated by XRD patterns and SEM observations (Figures S6,S8, Supporting Information), the adsorption ability improvement towards oil is mainly attributed to the combination of the increased interaction with the organic molecules because of the increase of lipophilicity and its unique open structure. As a result, rGGOM shows a decreased adsorption rate and capacity towards MB in water, as shown in Figure 3c. Most of the oxygen functional groups are removed after the reduction and the C/O ratios are about ≈ 8.1 for rGGOM and ≈14.4 for rGGOM-600, as indicated by the X-ray photoelectron spectroscopy (XPS) results shown in Figure S9, Supporting Information. A N1s peak is also detected due to the use of hydrazine hydrate as the reducing agent. Sheet resistance measurements using the four-probe method further demonstrate the reduction of the membranes, in which the resistances of rGGOM and rGGOM-600 are ≈30–40 $\Omega\ \square^{-1}$ and ≈2–3 $\Omega\ \square^{-1}$ respectively, suggesting the good conductivity of the reduced membranes. More importantly, the graphene layers are interconnected with each other, resulting in the low electron resistance in electrochemical applications.

From above discussion, we found the open structure endows the reduced membrane with high adsorption capability towards many molecules as well as the good conductivity, making it promising in various electrochemical applications. Another potential application of the strong adsorption capability is to restrict the dissolving of sulfur and the "shuttle effect" of the dissolved sulfur compounds in the cathode system of Li–S batteries. Various carbon nanostructures have been designed to wrap the sulfur particles to suppress polysulfide dissolution and "shuttle effect" while the conductivity is improved simultaneously. Although the obtained carbon-sulfur hybrid cathodes show acceptable electrochemical performance, these nanostructures are normally complicated and the preparation process is time-consuming and not suitable for wide applications.[13] Instead of constructing a very complicated wrapping structure, using the strong adsorption ability of this carbon material to confine the reaction intermediates and lithium polysulfide products on the electrode surface may be an easier strategy.[14] Considering the high adsorption ability and good conductivity of the rGGOM-600, it may be a potential carbon component for the carbon/sulfur cathode system. As expected, it also shows much higher adsorption ability towards sulfur and lithium polysulfides, and we therefore used it to confine sulfur for Li–S battery applications. A rGGOM-600/sulfur hybrid (sulfur fraction: 71 wt.% calculated from the TG curves shown in Figure S10a, Supporting Information) was prepared by a simple melt infiltration method and used as a cathode in a Li–S battery. The SEM images shown in Figure S10b demonstrate that the microstructure of the membrane is not changed and the elemental mapping of energy dispersive spectrometer (EDS) analysis (Figure S10c, Supporting Information) shows that the sulfur is uniformly distributed on the graphene sheets. The cyclic voltammetry (CV) profiles (Figure S11a, Supporting Information) clearly show two main cathode peaks at about 2.2 and 1.9 V in the first cycle because of the changes of S to Li polysulfides and the further reduction of higher-order Li polysulfides to Li sulfides, respectively. Only one anode peak appeared at about 2.55 V due to the high overvoltage induced conversion of Li_2S to Li polysulfides. In subsequent cycles, the main reduction and oxidation peaks shifted slightly. The typical discharge/charge profiles (Figure S11b, Supporting Information) show two plateaus, which are assigned to the two-step reaction of S with Li during discharge, in agreement with the CV profiles. Although the capacity of the hybrid at a low current density is lower than what has been reported somewhere, its rate performance and its capacity at a high current density are comparable to many of those with complex structures. It is noteworthy that the electrode shows excellent cycling performance, as shown in Figure 3d, and the capacity fade is negligible over 270 cycles, suggesting that the strong adsorption capability of the membrane effectively suppresses the dissolution of the polysulfides into the electrolyte during the charge/discharge process, while expanded graphite/sulfur hybrid as a reference shows poor electrochemical performance due to its weak adsorption capability. The cycled electrode was also characterized by the mapping of the EDS analysis (Figure S10d, Supporting Informatio), demonstrating that most of the sulfur is still adsorbed on the graphene nanosheets, indicating the obvious suppression of the "shuttle effect". Note that the contribution of graphene to capacity in the cathode system is neglectable, so the capacity is totally derived from the reaction of sulfur with Li. Although the capacity of rGGOM-600/sulfur hybrid is lower than those of nanomaterials with complex microstructures, it shows much stable cyclic ability and higher rate capability. Thus, it is remarkable for rGGOM-600/S hybrid because the achieved electrochemical performance is excellent with respect to such simple microstructure. Furthermore, it shows superior electrochemical performance to many hybrids prepared from the carbons with high surface area and complicated porous structure, such as ordered mesoporous carbons (Figure S12, Supporting Information). Considering the easy preparation process and the morphology which is easy to be handled, such membrane is still attractive in the future practical applications.

The above discussion has proven that the utilization and accessibility of the graphene layers are improved due to the open microstructure, which is also important to most of the electrochemical applications. In order to further prove the aforementioned advantages of the membrane, we characterized the supercapacitive performance of a membrane electrode. Note that the membrane can be used as an electrode directly without a collector, binders or conductive additives. **Figure 4**a shows the CV profiles of the membrane electrode in three electrode systems with a KOH solution as the electrolyte. A typical rectangular shape is observed at a low scanning rate for rGGOM and rGGOM-600 electrodes, indicative of good charge propagation at the electrode surface following

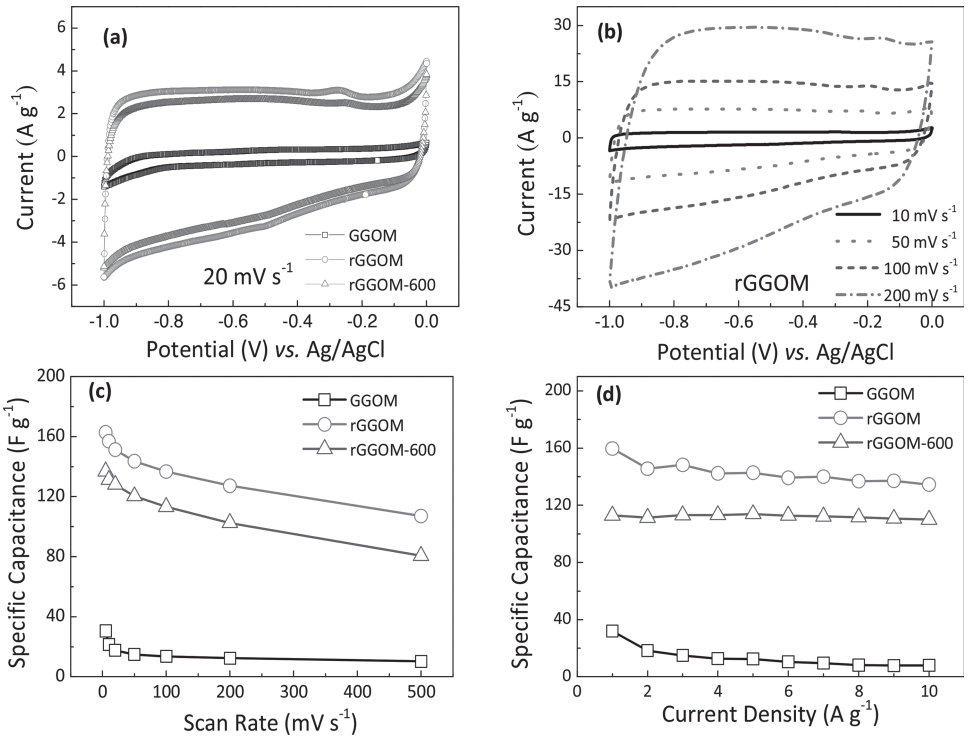

Figure 4. Electrochemical performance of membranes. a) CV profiles of GGOM and reduced GGOM at a scanning rate of 20 mV s^{-1} in KOH solution; b) CV profiles of rGGOM with different scanning rates; c) Specific capacity of GGOM and reduced GGOM for different scanning rates; d) Specific capacity of GGOM and reduced GGOM with different current densities.

the electric double layer charging mechanism. The electrochemical capacitance of GGOM is very low due to its poor conductivity caused by the absence of a reduction process. The open structure of the reduced membrane is characterized by low internal electron transport resistance and ion diffusion resistance indicated by the electrochemical impedance spectroscopy (EIS) as shown in Figure S13 (Supporting Information), which results in a small distortion of the CV curves at a high scanning rate (Figure 4b). Thus, high power capability is achieved with ≈64% and 68% capacitance retention for rGGOM and rGGOM-600 respectively, from scanning rates of 2 mV s^{-1} to 500 mV s^{-1}. rGGOM shows a higher capacitance than does rGGOM-600 that has substantially fewer functional groups (Figure 4c), which is in accordance with the previous reports.[15] Note that rGGOM shows a much higher capacitance compared to the reduced TGOM (Figure S14, Supporting Information) and the membrane electrode with tightly layered structure reported previously as expected,[16] and in these cases the tightly layered structure is not conducive for ion storage and transport. The capacitance and rate performance of rGGOM based on the two-electrode measurement also show similar results. A capacitance of about 120 F g^{-1} at the current density of 10 A g^{-1} (Figure S15, Supporting Information) is obtained, which is slightly lower than the results measured by three-electrode system. The capacitance of rGGOM was also measured in the organic electrolyte (1 M $(C_2H_5)_4NBF_4$/PC), which also shows acceptable capacitance and high rate performance (90 F g^{-1} under the current density of 10 A g^{-1} with the potential widow of 2.5 V). That is, in the graded structure in rGGOM, the compact layers on the top act as a collector, the middle, with an expanded and loosened structure is responsible for ion storage and the bottom with vertically aligned channels for fast ion transportation. Thus, it shows high power performance (Figure 4c,d) due to the open structure and high conductivity derived from the more integrated graphene layers. Meanwhile, it possesses similar capacitance as the graphene powders,[17] making it promising to be directly used as the electrode for high rate capacitors.

3. Conclusion

In conclusion, the control on the removal of water trapped between the stacked layers is found to have the ability to tune the layer stacking orientation and the microstructure of graphene oxide membrane, and inspired by the phase diagram of pure water, a fast water removal with a reduced pressure results in an instantaneous phase change across three phases and generates strong forces that pull the layers into a vertical orientation and promotes the formation of the open and graded microstructure. Thus, the resulting membrane has a much higher adsorption ability than a membrane with a closely stacked structure obtained by normal drying at atmospheric pressure. The strong adsorption ability is also found to be efficient in suppressing the "shuttle effect" of the polysulfide in the cathode system of a Li–S battery. Furthermore, the membrane

can be directly used as a membrane electrode and shows fast ion transport, revealing great potential in supercapacitors and other electrochemical applications. More efforts are on-going to precisely tune the graded microstructure, of which the thickness and layer orientation of different section are controlled, to optimize the electrochemical performance. This discovery provides us a new strategy based on the controlled removal process of the trapped water that can be developed as a tailoring method for the microstructure of not only graphene but also many other nanomaterials and their arranging state to cater for different applications.

4. Experimental Section

Assembly of the GGOM: Graphite oxide was first prepared from graphite power by a modified Hummers method as reported elsewhere.[15a] It was then subjected to strong sonication (200 W, JY92-N, a high-energy bench mounted ultrasonic disintegrator) in deionized water for 2 h to obtain a homogeneous GO hydrosol with a concentration of 2 mg mL^{-1}. The membrane was prepared by using a liquid/air interface self-assembly method proposed by our group.[8a] In a typical experiment, the GO hydrosol was heated at 80 °C for 30 min in a water bath with thermostatic control, during which a smooth and condensed membrane was formed at the liquid/air interface. Note that such an assembly period is suitable for the formation of GGOM, since the top layered structure cannot well formed in a shorter assembly period while the too long assembly period results in the much thicker top layered structure and decreased surface utilization. The wet membrane was then transferred onto a polytetrafluoroethene substrate and was quickly placed into a vacuum freeze drier (ALPHA 1–2 LDplus, Christ, Germany) for 24 h, and finally, the GGOM, which has an open texture and graded structure, was obtained.

Reduction of the GGOM: In order to maintain the membrane structure after reduction, a mild two-step reduction process was developed. In the first step, the GGOM was reduced using hydrazine hydrate vapor at 80 °C for 10 h to release most of the oxygen groups, and the obtained membrane is denoted as rGGOM. In order to further improve the reduction degree, rGGOM was treated at 600 °C for 4 h in Ar (99.999%) atmosphere. Due to the removal of functional groups in the first step, the membrane structure is slightly changed during the thermal treatment. The final reduced membrane is denoted rGGOM-600.

Preparation of the Membrane/Sulfur Hybrid: A melt impregnation method was used for the hybrid preparation.[13b] In a typical preparation process, rGGOM-600 and sulfur powders with a mass ratio of 3:7 were ground together and heated at 155 °C for 12 h in an argon atmosphere, during which all the molten sulfur was impregnated into the open texture of the membrane. Thermogravimetry (TG) analysis shows the sulfur fraction of the obtained hybrid is about 71% by weight (Figure S10a, Supporting Information). An expanded graphite/sulfur hybrid and ordered mesoporous carbon (CMK-3 with a specific surface area of 1000 $m^2\ g^{-1}$) /sulfur hybrid were prepared under the same conditions for comparison.

Structure Characterization: Scanning electron microscopy (SEM) observations were conducted with Hitachi S-4800 (Hitachi, Japan) equipped with an Energy Dispersive Spectrometer (EDS, Thermo Scientific, USA). The X-ray diffraction (XRD) measurements were collected at room temperature using the reflection mode (D8 FOCUS, Cu Kα radiation, λ = 0.154nm). The X-ray photoelectron spectroscopy (XPS) characterization of the products was performed on an Axis Ultra photoelectron spectrometer using an Al Kα (1486.7 eV) X-ray source. The square resistance measurements were obtained using a four-point probe method (ST-2258A, Suzhou Jingge Electronic Co., LTD, China). For each sample, the square resistance was obtained by averaging the measured values for five different positions. Nitrogen adsorption was measured by using a BEL mini-instrument, and the specific surface area was obtained by Brunauer-Emmett-Teller (BET) analyses of the adsorption isotherms. TG (Rigaku, Japan) measurement was performed (20–800 °C) with the heating rate of 5 °C min^{-1}.

Adsorption of Methylene Blue (MB): The GGOM can be tailored into a certain shape and directly used as a filtration membrane. Ultraviolet (UV)-visible (vis) spectroscopy (UV-1102, Techcomp, China) was used to characterize the concentration changes of MB before and after adsorption by the membrane. For adsorption kinetic measurement, the membranes were placed in 50 mL-falcon tubes containing the MB solutions of the same concentration, and the adsorption capacity for different adsorption periods were measured and calculated from the absorbencies by using a UV-vis spectrophotometer, and the adsorption rate was obtained by fitting the adsorption amount and the adsorption periods. The amount of MB adsorbed at equilibrium, q_e was calculated from the mass balance equation given by:

$$q_e = V\frac{C_0 - C_e}{m_s}$$

where C_0 and C_e (mg L^{-1}) are the initial and final concentrations of adsorbate in the flasks respectively. V is the volume of the solution (L), and m_s is the mass of dry adsorbent used (g).

Adsorption of Oil and Organic Molecules: The oil adsorption capacities of the membranes were determined by weight measurement. In a typical process, the membranes were first put into the oil and removed by tweezers after 30 minutes. After the residues on the outside surface were removed by filter paper, the adsorption capacity is calculated by the membrane weight differences before and after adsorption. The same measurements were also conducted for the adsorption capacity calculation of expanded graphite.

Electrochemical Performance of the Membrane/Sulfur Composite: For the electrode preparation, a rGGOM-600/sulfur hybrid membrane was used as the cathode to assemble a 2032 type coin cell in an Ar-filled glove box (MBraun Unilab) for measurement and a lithium metal foil was used as anode. The electrolyte was 1.0 M lithium bis(trifluoromethanesulfonyl) imide (LiTFSI) in 1, 3-dioxolane (DOL) and 1, 2-dimethoxyethane (DME) (1:1 by volume) with 0.5 wt% $LiNO_3$ additive. Galvanostatic charge-discharge profiles and the cyclic performance were tested using a Land electrochemical instrument (PCBT-100–32D, Wuhan Lixing, China), and the cyclic voltammetry (CV) measurements were conducted using an electrochemical workstation (VMP3, Bio-Logic, France). The current density set for cell testing referred to the mass of sulfur in the cathode and varied from 0.3 A g^{-1} to 6 A g^{-1}. The charge–discharge voltage range was selected from 1.5 V to 2.8 V versus Li^+/Li.

Electrochemical Performance of the Membrane Electrode for a Supercapacitor in Three-Electrode and Two-Electrode Systems: The membranes were tailored to a size of 10 mm × 5 mm with a weight of ≈0.5 mg and were directly used as the working electrode. In the measurement, the membrane working electrode was connected to a stainless steel mesh which used as a conductivity wire by silver paste, and a slice of platinum and a Ag/AgCl electrode were used as the counter electrode and reference electrode, respectively. 30 wt% KOH aqueous solution was used as the electrolyte. CV and electrochemical impedance spectroscopy (EIS) measurements were conducted using an electrochemical workstation (VMP3, Bio-Logic), and the EIS measurements were tested in the frequency range from 100 kHz to 10 mHz at an open-circuit potential with an AC perturbation of 5 mV. The capacitance based on two-electrode system was measured by assembling a symmetrical capacitor with KOH or $(C_2H_5)_4NBF_4$/PC (1 M) as electrolyte, and calculated by using galvanostatic charge–discharge results.

Supporting Information

Supporting Information is available from the Wiley Online Library or from the author.

Acknowledgements

W.L., Z.J.L., and G.M.Z. contributed equally to this work. This work was supported by the National Basic Research Program of China (2014CB932403), National Science Foundation of China (No. 51232005, 51372167 and 51302146), NSF of Tianjin, China (No. 12JCZDJC27400) and Shenzhen Basic Research Project (No. JC201104210152A and JCYJ20130402145002430), China Postdoctoral Science Foundation (2012M520012 and 2013T60111). The authors thank the financial support from Guangdong Province Innovation R&D Team Plan (No. 2009010025). The authors also thank Dr. Zhe Weng for his kind help in supercapacitor assembly and measurements.

Received: December 3, 2013
Revised: January 1, 2014
Published online: February 24, 2014

[1] a) D. A. Dikin, S. Stankovich, E. J. Zimney, R. D. Piner, G. H. B. Dommett, G. Evmenenko, S. T. Nguyen, R. S. Ruoff, *Nature* **2007**, *448*, 457; b) K. S. Kim, Y. Zhao, H. Jang, S. Y. Lee, J. M. Kim, K. S. Kim, J. H. Ahn, P. Kim, J. Y. Choi, B. H. Hong, *Nature* **2009**, *457*, 706; c) R. R. Nair, H. A. Wu, P. N. Jayaram, I. V. Grigorieva, A. K. Geim, *Science* **2012**, *335*, 442; d) F. Liu, S. Y. Song, D. F. Xue, H. J. Zhang, *Adv. Mater.* **2012**, *24*, 1089; e) H. Chen, M. B. Muller, K. J. Gilmore, G. G. Wallace, D. Li, *Adv. Mater.* **2008**, *20*, 3557.

[2] a) M. F. El-Kady, V. Strong, S. Dubin, R. B. Kaner, *Science* **2012**, *335*, 1326; b) W. Gao, N. Singh, L. Song, Z. Liu, A. L. M. Reddy, L. J. Ci, R. Vajtai, Q. Zhang, B. Q. Wei, P. M. Ajayan, *Nat. Nanotechnol.* **2011**, *6*, 496; c) X. Zhao, C. M. Hayner, M. C. Kung, H. H. Kung, *ACS Nano* **2011**, *5*, 8739; d) J. J. Shao, W. Lv, Q. G. Guo, C. Zhang, Q. Xu, Q. H. Yang, F. Y. Kang, *Chem. Commun.* **2012**, *48*, 3706.

[3] J. J. Yoo, K. Balakrishnan, J. S. Huang, V. Meunier, B. G. Sumpter, A. Srivastava, M. Conway, A. L. M. Reddy, J. Yu, R. Vajtai, P. M. Ajayan, *Nano Lett.* **2011**, *11*, 1423.

[4] X. W. Yang, L. Qiu, C. Cheng, Y. Z. Wu, Z. F. Ma, D. Li, *Angew. Chem. Int. Ed.* **2011**, *50*, 7325.

[5] a) Z. Q. Niu, J. Chen, H. H. Hng, J. Ma, X. D. Chen, *Adv. Mater.* **2012**, *24*, 4144; b) C. M. Chen, Q. Zhang, C. H. Huang, X. C. Zhao, B. S. Zhang, Q. Q. Kong, M. Z. Wang, Y. G. Yang, R. Cai, D. S. Su, *Chem Commun* **2012**, *48*, 7149; c) H. C. Gao, F. Xiao, C. B. Ching, H. W. Duan, *ACS Appl. Mater. Interfaces* **2012**, *4*, 2801; d) J. J. Shao, S. D. Wu, S. B. Zhang, W. Lv, F. Y. Su, Q. H. Yang, *Chem. Commun.* **2011**, *47*, 5771.

[6] a) L. Qiu, J. Z. Liu, S. L. Y. Chang, Y. Z. Wu, D. Li, *Nat Commun* **2012**, *3*; b) X. W. Yang, C. Cheng, Y. F. Wang, L. Qiu, D. Li, *Science* **2013**, *341*, 534.

[7] Y. Tao, X. Y. Xie, W. Lv, D. M. Tang, D. B. Kong, Z. H. Huang, H. Nishihara, T. Ishii, B. H. Li, D. Golberg, F. Y. Kang, T. Kyotani, Q. H. Yang, *Sci. Rep.* **2013**, *3*, 2975.

[8] a) C. M. Chen, Q. H. Yang, Y. G. Yang, W. Lv, Y. F. Wen, P. X. Hou, M. Z. Wang, H. M. Cheng, *Adv. Mater.* **2009**, *21*, 3007; b) W. Lv, Z. X. Xia, S. D. Wu, Y. Tao, F. M. Jin, B. H. Li, H. D. Du, Z. P. Zhu, Q. H. Yang, F. Y. Kang, *J Mater. Chem.* **2011**, *21*, 3359; c) S. D. Wu, W. Lv, J. Xu, D. Han, X. Chen, P. Wang, Q. H. Yang, *J. Mater. Chem.* **2012**, *22*, 17204.

[9] H. C. Bi, K. B. Yin, X. Xie, J. Ji, S. Wan, L. T. Sun, M. Terrones, M. S. Dresselhaus, *Sci. Rep.* **2013**, *3*, 2714.

[10] W. L. Li, K. Lu, J. Y. Walz, *Int. Mater. Rev.* **2012**, *57*, 37.

[11] J. M. Dias, M. C. M. Alvim-Ferraz, M. F. Almeida, J. Rivera-Utrilla, M. Sanchez-Polo, *J. Environ. Manage.* **2007**, *85*, 833.

[12] Y. Zhao, C. G. Hu, Y. Hu, H. H. Cheng, G. Q. Shi, L. T. Qu, *Angew. Chem. Int. Ed.* **2012**, *51*, 11371.

[13] a) L. W. Ji, M. M. Rao, H. M. Zheng, L. Zhang, Y. C. Li, W. H. Duan, J. H. Guo, E. J. Cairns, Y. G. Zhang, *J. Am. Chem. Soc.* **2011**, *133*, 18522; b) D. W. Wang, G. M. Zhou, F. Li, K. H. Wu, G. Q. Lu, H. M. Cheng, I. R. Gentle, *Phys. Chem. Chem. Phys.* **2012**, *14*, 8703; c) G. M. Zhou, D. W. Wang, F. Li, P. X. Hou, L. C. Yin, C. Liu, G. Q. Lu, I. R. Gentle, H. M. Cheng, *Energy Environ. Sci.* **2012**, *5*, 8901; d) W. Y. Li, G. Y. Zheng, Y. Yang, Z. W. Seh, N. Liu, Y. Cui, *Proc. Natl. Acad. Sci. U. S. A.* **2013**, *110*, 7148; e) G. Zhou, S. Pei, L. Li, D. W. Wang, S. Wang, K. Huang, L. C. Yin, F. Li, H. M. Cheng, *Adv. Mater.* **2013**.

[14] M. S. Song, S. C. Han, H. S. Kim, J. H. Kim, K. T. Kim, Y. M. Kang, H. J. Ahn, S. X. Dou, J. Y. Lee, *J. Electrochem. Soc.* **2004**, *151*, A791.

[15] a) W. Lv, D. M. Tang, Y. B. He, C. H. You, Z. Q. Shi, X. C. Chen, C. M. Chen, P. X. Hou, C. Liu, Q. H. Yang, *ACS Nano* **2009**, *3*, 3730; b) C. Zhang, W. Lv, X. Y. Xie, D. M. Tang, C. Liu, Q. H. Yang, *Carbon* **2013**, *62*, 11.

[16] G. K. Wang, X. Sun, F. Y. Lu, H. T. Sun, M. P. Yu, W. L. Jiang, C. S. Liu, J. Lian, *Small* **2012**, *8*, 452.

[17] a) M. D. Stoller, S. J. Park, Y. W. Zhu, J. H. An, R. S. Ruoff, *Nano Lett.* **2008**, *8*, 3498; b) Y. W. Zhu, S. Murali, M. D. Stoller, A. Velamakanni, R. D. Piner, R. S. Ruoff, *Carbon* **2010**, *48*, 2118.